Journal of Natural Gas Science and Engineering 77 (2020) 103268

Contents lists available at ScienceDirect

Journal of Natural Gas Science and Engineering

journal homepage: http://www.elsevier.com/locate/jngse

Explicit tracking of CO_2-flow at the core scale using micro-Positron Emission Tomography (μPET)

Bergit Brattekås *, Malin Haugen

Department of Physics and Technology, University of Bergen, Norway

ARTICLE INFO

Keywords:
In-situ imaging
CO_2 flow
Carbonates
Explicit tracking of CO_2
Positron emission tomography

ABSTRACT

Safe subsurface sequestration of carbon dioxide (CO_2) is becoming increasingly important to meet climate goals and curb atmospheric CO_2 concentrations. The world-wide CO_2 storage capacity in carbonate formations is significant; within deep, saline aquifers and through several CO_2-enhanced oil recovery projects, with associated CO_2 storage. Carbonates are complex, both in terms of heterogeneity and reactivity, and improved core scale and sub core-scale analysis of CO_2 flow phenomena is necessary input to simulators, aiming to establish large-scale behavior. This paper presents a recent advancement in *in-situ* imaging of CO_2 flow, utilizing high-resolution micro-Positron Emission Tomography and radioactive tracer [^{11}C]arbon dioxide to explicitly track CO_2 during dynamic flow and subsequent trapping at the core scale. Unsteady state water injection (imbibition) and CO_2 injection (drainage) were performed in a low-permeable chalk core at elevated pressure conditions. Short-lived radioisotopes were used to label water and CO_2, respectively, and facilitated explicit tracking of each phase separately during single phase injection. Local flow patterns and dynamic spatial fluid saturations were determined from *in-situ* imaging during each experimental step. Initial miscible displacement revealed displacement heterogeneities in the chalk core, and dynamic image data was used to disclose and quantify local permeability variations. Radial permeability variations influenced subsequent flow patterns, where CO_2 predominantly flooded the higher-permeability outer part of the core, leaving a higher water saturation in the inner core volume. Injection of water after CO_2 flooding is proposed to be the most rapid and effective way to ensure safe storage, by promoting capillary trapping of CO_2. PET imaging showed that presence of CO_2 reduced the flow of water in higher-permeability areas, improving sweep efficiency and promoting a nearly ideal core-scale displacement. Alternate injections of water and gas is also expected to improve sweep efficiency and contribute to improved oil recovery and CO_2 storage on larger scales. Sub-core analysis showed that residually trapped CO_2 was evenly distributed in the chalk core, occupying 40% of the pore volume after ended water injection. Micro-Positron Emission Tomography yielded excellent small-scale resolution of both water and CO_2 flow, and may contribute to unlocking fluid flow dynamics and determining mechanisms on the millimeter scale; presenting a unique opportunity in experimental core-scale evaluations of CO_2 storage and security.

1. Introduction

Today there is little doubt that global warming is related to the increased CO_2 concentrations in the atmosphere. In the Paris Agreement from 2015 (COP21 Paris), the international community agreed to climate and energy goals limiting global warming to well below 2 °C above pre-industrial levels. Carbon capture, utilization and storage (CCUS) is identified as an important part of the portfolio of technologies needed to achieve these goals (IEA, 2019).

CO_2 can be injected in (active or depleted) hydrocarbon reservoirs, saline aquifers or non-mineable coal beds for long-term subsurface storage. Saline aquifer storage of CO_2 mostly targets sandstone formations, however; CO_2 injection to achieve enhanced oil recovery (EOR) is performed in several carbonate formations. Worldwide, more than 60% of proven oil reserves and 40% of gas reserves are found in carbonate formations (Akbar et al., 2000); hence a significant potential for CO_2 storage exist within carbonates. Carbonates represent complex flow systems, with fractures, small-scale heterogeneities and a wide range of pore sizes, in addition to being highly reactive (hence, dissolution may occur in parts of the formation during CO_2 injection due to

* Corresponding author.
E-mail address: bergit.brattekas@uib.no (B. Brattekås).

https://doi.org/10.1016/j.jngse.2020.103268
Received 20 December 2019; Received in revised form 17 February 2020; Accepted 17 March 2020
Available online 18 March 2020

acidification). Advanced laboratory methods are necessary to capture the properties of flow on the core and sub-core scales in such systems, to further map the controlling mechanisms of CO_2 storage in carbonate formations. In this paper we used micro-Positron Emission Tomography (μPET) to explicitly evaluate dynamic saturation development during brine and CO_2 injections in chalk at the core and sub-core scale. PET imaging, although primarily used in medicine and pre-clinical research as a diagnostic tool, is an up-and-coming imaging technology in porous media research. PET imaging is non-invasive and independent of experimental pressure and temperature conditions, and has high temporal and spatial resolutions at high signal to noise ratios. Recent advances in the imaging tool has spurred researchers to explore the limitations and possibilities associated with PET imaging during dynamic fluid flow in porous media (Kulenkampff et al., 2008; Fernø et al. 2015a, 2015b; Zahasky et al., 2019).

In-situ imaging has been extensively used to image fluid flow dynamics on the core scale, and the most used imaging modalities are Magnetic Resonance Imaging (MRI) and Computed Tomography (CT). MR imaging relies on spin detection from hydrogen atoms, and as such detects hydrogen-rich fluid phases, e.g. water and oil. MR imaging may implicitly monitor CO_2 injection by detecting the decrease in signal during injection into a core already saturated by water and/or oil (Ersland et al., 2010; Almenningen et al., 2018). CT monitors saturation based on attenuation measurements, and produce spatial representations of density contrasts through a porous medium. When the density contrast between injected and displaced fluids is high (e.g. between water and gas), CT may provide accurate and fast imaging at high resolution (Akin and Kovscek, 2003). CT or MR imaging also capture static rock structures, thus fluid flow behavior may be coupled with small scale heterogeneities in the core material. PET imaging represents an opportunity to image fluid flow without signal influence from the surrounding porous medium, and is often used in combination with CT or MRI. PET imaging only detects fluids labelled by positron-emitting radionuclides: in which emitted positrons will combine with an electron to balance atomic charge, and consequently send out photons of 511 keV energy in opposite directions. Annihilation events are detected by measuring photon coincidences versus time: to facilitate three-dimensional imaging, a ring consisting of several small detector elements encloses the porous medium. Post processing of the PET signal determine the position of each annihilation event in three dimensions, with high spatial and temporal accuracy. PET imaging, hence, offers the opportunity to visualize and quantify fluid flow *in-situ* at the core and local scale without signal influence from mineralogy, rock properties and initial saturation state. A range of radioisotopes are available for explicit labelling of different fluid phases, and new radioisotopes are continuously being developed: radioactive isotope ^{11}C–CO_2 facilitates explicit detection of CO_2 within the porous medium by PET imaging. Explicit quantification of CO_2 behavior is helpful for determining the potential of a storage formation, e.g. by measuring caprock capillary threshold pressure (Fernø et al., 2015a demonstrated that PET imaging could be used to determine CO_2 entry into very low-permeable shale), and porous media flow parameters including CO_2/brine relative permeability: parameters that are necessary input for numerical simulators and must be measured in controlled core-scale experiments (Busch and Müller, 2011).

The spatial resolution of PET imaging is limited by several parameters, including the distance between the annihilation event and the PET detector elements, and the area of the detector elements (Levin and Hoffman, 1999; Bailey et al., 2005; Zahasky et al., 2019). Small pre-clinical μPET scanners have been proposed to yield optimum resolution, and was previously used to investigate spontaneous imbibition (Ruth et al., 2016; Føyen et al., 2019), dynamic wormholing phenomena (Brattekås et al., 2017), fracture flow diversion by polymer gel (Brattekås and Seright, 2018), foam generation and flow in natural fracture networks (Brattekås et al., 2019) and single-and multiphase transport parameters during water and nitrogen gas injection in sandstone (Zahasky and Benson, 2018). μPET imaging was previously performed using the most common radioisotope for fluid flow studies: Fluorodeoxyglucose (^{18}F) (comprehensive overview may be found in Zahasky et al. (2019). ^{18}F may be dissolved in water, and can therefore be used for explicit imaging of water flow, and implicit imaging of other fluids by quantifying the loss of signal over time. The half-life (time it takes to decrease the original level of radioactivity to 50%) of ^{18}F is 109 min. Radioisotope ^{11}C, used to label CO_2, has a short half-life of 20 min, which pose additional experimental challenges; by limiting the time scale of experiments significantly, and in terms of safety regulations when handling high doses of radiation and produced radioactive gas. ^{11}C–CO_2 flow imaged by PET is therefore limited to only two previous studies: Fernø et al. (2015a) utilized ^{11}C to trace supercritical CO_2 propagation into shale at reservoir conditions, and Pini et al. (2016) mixed ^{11}C in an aqueous sodium bicarbonate solution to evaluate solute transport in a sandstone core at ambient conditions. Here we present, for the first time, explicit imaging of ^{11}C–CO_2 propagation into a chalk core at elevated pressure conditions, imaged by μPET. Alternate water and gas injections were performed, where each fluid was explicitly imaged during injection. Brine was labelled using ^{18}F, and CO_2 was labelled using ^{11}C. The signal of brine or gas was allowed to decay before the next injection, in the following cycle: ^{18}F-brine → ^{11}C–CO_2 → ^{18}F-brine. Spatial fluid saturations were calculated based on the registered activity of the labelled brine or gas phase at given time steps. Dynamic *in-situ* imaging presents an addition to global measurements, to more accurately determine local flow properties. This is particularly useful during unsteady-state experiments involving water/CO_2, where the results may be strongly influenced by heterogeneity, viscosity contrasts (fingering) and end effects (Busch and Müller, 2011).

2. Materials and methods

2.1. Preparations of the core and experimental set-up

A compact experimental setup (Fig. 1) was built to facilitate quick and safe imaging of high-pressure fluid injections in a CT 80 W Nanoscan PC imager μPET scanner. The setup was designed to minimize the risks for leakage, by reducing the number of connections and valves. The experimental set-up consisted mainly of: three piston pumps, a core holder, a back-pressure regulator, and several in-line pressure transducers, and is further described below.

A cylindrical Rørdal chalk core (Ekdale and Bromley, 1993) with 3.81 cm diameter and 8.44 cm length was washed and dried at elevated temperature. The core was fully saturated by brine (5 wt%NaCl, 5 wt% $CaCl_2$) under vacuum and the porosity was determined by weight measurements ($\varphi = 46.5\%$). Absolute permeability (K) was measured by injecting brine into the core at different volumetric flow rates while measuring the differential pressure across the core, and was calculated by Darcy's law [Eq. (1)] to 6.15 mD.

$$K = \frac{Q\mu L}{A\Delta P} \quad [1]$$

Eq. (1) gives a generalized form of Darcy's law, applicable to horizontally aligned, fully saturated and uniformly shaped porous media, such as the chalk core plug. All parameters on the right side of the equation are measured directly in the laboratory: the length (L) and cross-sectional area (A) of the core plug, and the pressure drop across the core (ΔP) during injection of an incompressible fluid, with a constant viscosity (μ) at different volumetric flow rates (Q).

The core was wrapped in aluminum foil and placed in a Viton sleeve with 1.5″ peek end pieces at each end. Distribution grooves in the end pieces ensured a uniform distribution of fluids across the core cross section during injections. The core was mounted in a custom-made core holder certified to 200 bar pressure (©RS Systems, Trondheim, Norway). Pump 3 (ISCO piston pump) contained light mineral oil and was used to apply and maintain confinement pressure around the core, held 10 bar above the line pressure for the duration of the experiment. The core

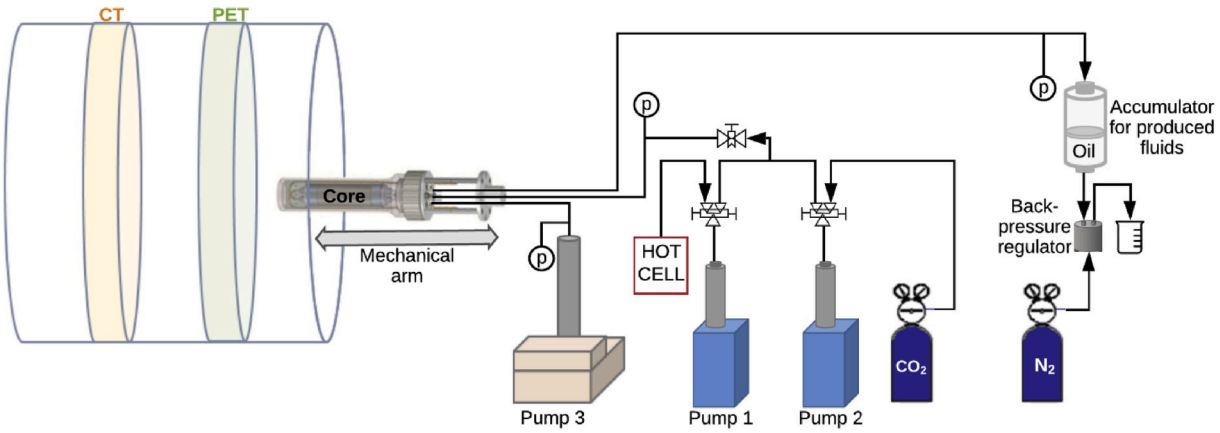

Fig. 1. Schematic of the experimental setup used for PET imaging of radiolabeled CO_2 and brine injections. Pump 1 was used to inject brine into the core, and also received $^{11}C–CO_2$ in gaseous state from the hot cell, and was used to inject CO_2 into the core. Pump 2 contained pressurized CO_2. Produced fluids were collected in an accumulator. The system pressure was controlled by a back-pressure regulator connected to a nitrogen tank. Line pressures (P) were measured using pressure gauges connected to the injection and production lines. Confining pressure was controlled by Pump 3. The mechanical arm moves the core holder horizontally into position for CT and PET imaging.

holder was attached to a mechanical arm outside the μPET scanner. The mechanical arm is controlled through the scanner software (©Nucline), and moves the core holder horizontally into the position determined by the operator. The core holder must be able to move freely along the z-axis to be positioned within the field of view detectable by μPET imaging. The core holder was therefore connected to flexible peek injection and production lines. The injection line was connected to two piston pumps (Sanchez Technologies): Pump 1 and 2 were connected by 1/8″ Hastelloy tubing (Swagelok) facilitating valves (Autoclave) and could easily be isolated from each other and/or the core system. Liquid ^{18}F-FDG was received before each water injection, and was mixed with brine and pressurized in Pump 1. Before CO_2 injection, Pump 1 was connected to the hot cell using 1/8″ plastic Swagelok tubing, and the radioactive isotope was transferred directly into the pump at a slightly elevated pressure (≈ 8 bar). $^{11}C–CO_2$ was mixed and pressurized to experimental conditions in the pump by transferring pressurized CO_2 from Pump 2. Radioactively labelled brine or CO_2 was injected from Pump 1 into the common, flexible injection line. The production line was connected to a piston accumulator, filled with mineral oil. The radioactive fluid was collected on the top side of the piston. Oil was produced at the lower end of the accumulator, which was connected to a back-pressure regulator controlled by a Nitrogen gas tank. The core system was pressurized to 68 bars by non-labelled brine before labelled injection started. Initial CT scans were acquired to determine the position of the core, and the core holder was thereafter moved into the PET field of view, ranging 8*8*9.47 cm in the x-, y-, z-directions. PET sequences were acquired, where the spatial resolution offered by the detector system was 0.4 mm^3. Three radiolabeled floods were monitored using PET acquisitions: the injection procedure for each flood is detailed in section 2.2.

2.2. Fluid injections

1st brine injection: Radioactively labelled brine was injected into the chalk core to miscibly displace the initial brine saturation and determine inherent displacement heterogeneities within the core. ^{18}F was produced by a local cyclotron and used to synthesize ^{18}F-fluorodeoxyglucose (^{18}F-FDG), which is a water-soluble fluorine radioisotope with a half-life of 109 min 350 MBq of ^{18}F-FDG was received in a syringe and mixed in brine (5 wt%NaCl, 5 wt%$CaCl_2$). The brine was transferred to the injection pump (Pump 1, Fig. 1) and pressurized to the experimental conditions. Pump 2 contained pressurized CO_2 and was not used during this stage. PET acquisition was performed while radioactive brine was injected into the core at a volumetric flow rate of 1 cm^3/min. Two pore volumes (PV) of brine were injected, and the core pore volume remained fully saturated by water during this flood. The back-pressure was kept constant at 68 Bar. After water injection, the core was shut-in and remaining radioactivity allowed to decay before further injections.

CO_2 injection: 2 PV of $^{11}C–CO_2$ was injected into the chalk core. Water was displaced by CO_2, thus the volume of water in the pore volume decreased and the volume of gas increased. When several immiscible fluids are present in the same pore space, their respective volumes are often expressed as saturation, S_i, which describes the fraction of the total pore volume filled with a fluid i. When gas invaded the chalk core, the fraction of water in the pore volume decreased from $S_w = 1$ (pore volume 100% water filled), to a lower, irreducible water saturation, S_{wi}. The gas saturation in the pore volume increased correspondingly, and could be explicitly quantified by PET imaging. Pump 1 was emptied and set to receive while [^{11}C]arbon dioxide was produced by the cyclotron and transferred at an elevated pressure through nylon tubings directly into the pump. 2 GBq of $^{11}C–CO_2$ was pressurized in Pump 1 by transferring 350 cm^3 of pre-pressurized CO_2 from Pump 2. Radioactive CO_2 was injected from Pump 1 into the chalk core using a volumetric injection rate of 1 ml/min, while the fluid distribution was continuously recorded by PET. The experimental pressure condition was 50 bars, thus CO_2 was compressed by a factor of 79 compared to atmospheric conditions and injected in vapor phase. After 2 PV of CO_2 had been injected, the core was shut in and $^{11}C–CO_2$ decayed swiftly. A second injection of ^{18}F-FDG labelled water was performed within a few hours.

2nd brine injection: Water was injected to promote capillary trapping of CO_2. ^{18}F- FDG labelled brine displaced CO_2 to the residual gas saturation (the fraction of the pore volume filled with water increased, and the fraction filled with gas decreased to a lower, immobile value, S_{gr}, which correspond to the volume of capillary trapped CO_2). The procedure was similar to the first brine injection; 350 MBq of ^{18}F-FDG was mixed in brine, pressurized to the experimental pressure condition (50 Bar, similar to CO_2 injection) and injected using a volumetric flow rate of 1 ml/min. The spatial distribution of fluids was continuously monitored by PET acquisitions.

2.3. Post-processing and analysis of in-situ saturations

Post-processing of the PET signal was necessary to determine the saturation and spatial distribution of each fluid. Three-dimensional PET images were reconstructed, where each image frame represented a time span of 5 min. It must be acknowledged that high volumetric injection rates coupled with long reconstruction frames implement a higher uncertainty in the images, in terms of localizing of the displacement front. For the purpose of this paper, the uncertainty was tolerable (within 6%

of the pore volume). Post-processing of the PET signal may be performed several times, using different time intervals. The images were reconstructed without attenuation correction from CT. Spatial fluid saturations could then be calculated based on the registered activity of the labelled brine or gas phase.

The three-dimensional core images were further sub-divided into sub-core sections, to evaluate discrepancies from ideal displacement that were observed during the first brine and CO_2 injections. Pini et al. (2016) and Zahasky and Benson (2018) previously performed sub-core scale analysis based on three-dimensional (3D) PET-data, where the core was subdivided into streamline tubes spanning the full core length, essentially collapsing three-dimensional saturation data to a two-dimensional (2D) bundle of tubes. The necessary assumptions for such sub-division, in addition to similar pressure boundary conditions for all tubes, is that flow within each element is one-dimensional with constant velocity, and that mixing or transverse dispersion between the tubes do not occur. Dynamic fluid flow data during water and gas injections showed that the best option to collapse the present 3D data to 2D was by sub-dividing the core into concentric shells (Fig. 2), due to a clear radial difference in the displacement. Four concentric shells were implemented on the core cross-section, at nine different core lengths.

3. Results and discussion

3.1. 1st brine injection

Miscible ^{18}F-FDG labelled brine injection (at $S_w = 1$), was first performed, where PET imaging revealed displacement heterogeneities within the chalk core (Fig. 3). Water breakthrough occurred at t = 0.67 PV water injected, hence the displacement deviated from ideal displacement, where the water breakthrough is anticipated to occur at 1 PV injected. Visualization by PET showed that the injected brine moved faster close to the core circumference, with a swift breakthrough at the production end.

PET visualization (Fig. 3) showed that the increase in radiolabeled water saturation was slower in the inner part of the core compared to the core circumference. Sub-core analysis was used to identify the cause for deviation from ideal displacement during miscible brine-brine displacement (Fig. 4): The accumulated volume of radiolabeled water ($V_{FDGbrine}$) across the core length increased linearly in all concentric shells before water breakthrough. Core scale development was near ideal (displaced volumes equal to displaced, as expected) with a faster development in the outer core region (Shell 4) and a slower development in the inner core (Shell 1, 2 and 3). The partial volume flow in each concentric shell could be determined from the slope of each line in Fig. 4, and Darcy's law was used to determine absolute sub-core permeabilities to 4.4 mD (inner core, Shell 1), 4.8 mD (Shell 2), 5.6 mD (Shell 3) and 7.1mD (core circumference, Shell 4). The permeability variation significantly impacted the water displacement. Further, each of the nine core positions were analyzed separately. Fig. 4 (right side) summarize the findings by showing two separate core positions; dimensionless length (Xd) 0.15 and 0.57. Displacement discrepancies between inner and outer core regions was more pronounced when the displacement front advanced further from the inlet, yielding a much slower development in core center saturation at higher X_d. The PET signal reached the same end point in all shells, which indicates that the pore volume of water is not spatially dissimilar-i.e. the porosity does not vary significantly within the core. Permeability variations can, hence, not be attributed to porosity directly. Pore size variations could cause a variation in permeability, but may not be determined by PET imaging. Rørdal chalk core material is expected to be relatively homogeneous; because globally measured porosity and permeability values are within the expected range, deviations from ideal displacement would not be determined (or expected) without *in-situ* imaging.

3.2. CO_2 injection

Radiolabeled CO_2 was injected into the core, reducing the water saturation towards irreducible (S_{wi}). Displacement heterogeneities were further amplified during CO_2 injection (Fig. 5), due to the unfavorable mobility ratio of gaseous CO_2 displacing higher-viscosity brine. CO_2 breakthrough was recorded at the production end after 0.5 PV injected. The average CO_2 saturation at the end point was calculated from the ^{11}C–CO_2 intensity to be 0.66, corresponding to an irreducible water saturation of 0.44. Quantitative core scale profiles (Fig. 5) show a clear gradient in saturation along the core length; with a significantly higher CO_2 saturation (i.e. higher signal) close to the inlet than further into the core. The CO_2 saturation range was measured to vary between 0.56 (close to the production end) and 0.87 (close to the inlet).

Sub-division of the core into sub-core concentric shells, as illustrated in Fig. 2, was performed. A gradient in CO_2 intensity (i.e. saturation) along the core length was also clearly visible in the sub-core analysis (Fig. 6), where the saturation end-points were significantly lower further into the core (X_d 0.57), than close to the inlet (X_d 0.15). A second, radial, gradient in CO_2 saturation was also revealed: although the CO_2 saturation increased in all shells, the saturation development was slower in the inner parts of the core (yellow lines in Fig. 6) compared to the outer parts of the core (blue lines in Fig. 6). Longitudinal and radial displacement discrepancies led to a poorer drainage by CO_2 in the core center and close to the production end. The core was shut-in after injection, and the signal from ^{11}C–CO_2 decayed.

3.3. 2nd brine injection

Radiolabeled brine was injected a second time to facilitate residual trapping of CO_2. PET imaging revealed an even displacement of CO_2 from the pore space, with no significant radial or longitudinal variations on the core or sub-core scale (Fig. 7). The water saturation at breakthrough averaged 0.60, hence capillary trapped CO_2 occupies 40% of the pore volume. The signal end points reached in each concentric shell

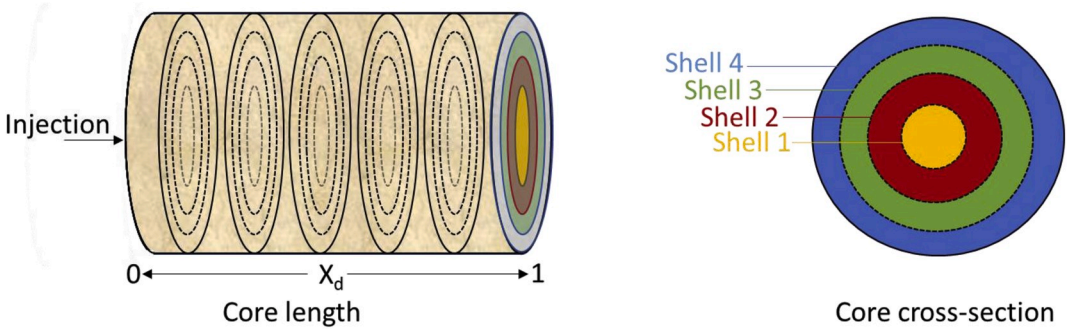

Fig. 2. Sub-core analysis was performed by dividing the core cross-section into concentric shells. Four concentric shells were analyzed in the axial direction, for nine different core lengths i.e. each cross-section represented 1 cm of the core. Dimensionless core length (X_d) was used.

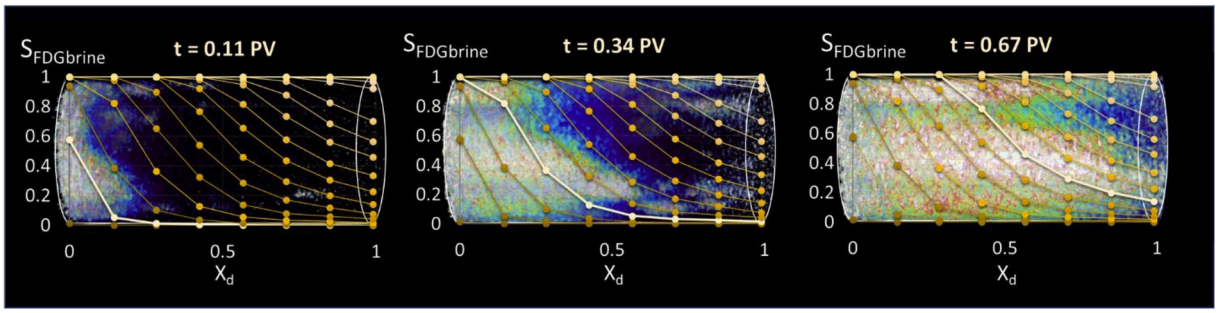

Fig. 3. Development of miscible FDG brine-brine displacement in a cylindrical chalk core sample. Qualitative 3D images of core saturation are overlaid by quantitative 1D profiles derived from the PET signal. In the three-dimensional images, bright colors correspond to a strong PET signal (high number of annihilation events). Three different time steps are shown: t = 0.11PV (left), t = 0.34 PV (middle) and t = 0.67 PV (right). Injected water broke through at the production end at t = 0.67 PV, due to flow heterogeneities.

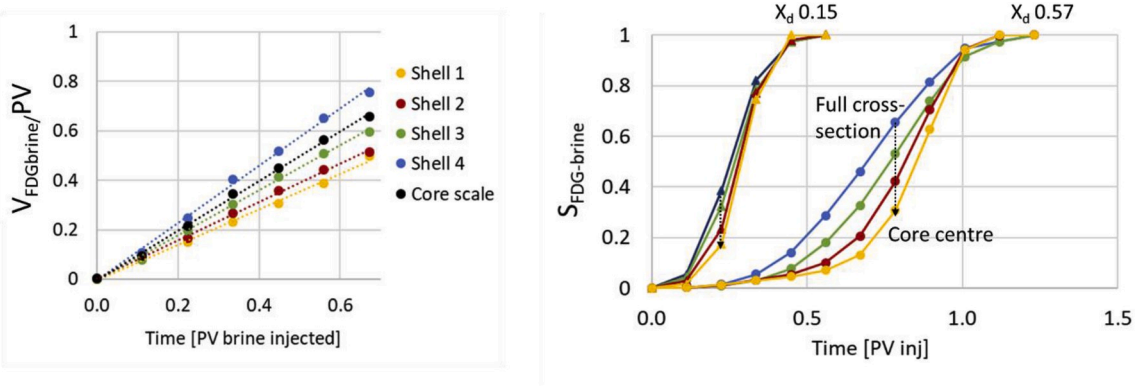

Fig. 4. Volume of radiolabeled water (V_w) in each concentric shell as a function of time (left). A linear displacement was seen in all core regions, with faster increase in the outer core (Shell 4), caused by a higher permeability. V_w was normalized to the pore volume, which gives water saturation. Dimensionless core lengths 0.15 and 0.57 are shown separately on the right, and emphasize that displacement discrepancies are more pronounced further into the core. The core was fully saturated by water at the end of injection, thus the same endpoint signal was reached in all shells.

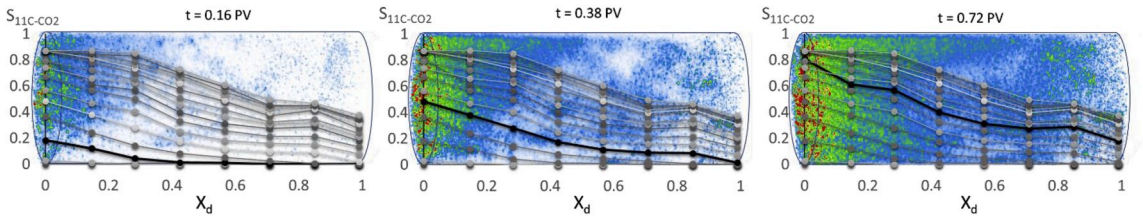

Fig. 5. Dynamic saturation development during $^{11}C–CO_2$ injection into a chalk core. Qualitative 3D images of core saturation are overlaid by quantitative 1D profiles derived from the PET signal. Three different time steps are shown: t = 0.16 PV (left), t = 0.38 PV (middle) and t = 0.72 PV (right). Injected CO_2 broke through at the production end at t = 0.5 PV, due to flow heterogeneities and an unfavorable mobility ratio. In the 3D images, red color represents the highest PET intensity (seen immediately after the inlet at t = 0.38 and t = 0.72), followed by green and blue. Areas with no signal from $^{11}C–CO_2$ are shown in white. -The mixed white/blue color close to the production end at t = 0.72 PV indicates large spatial variations in CO_2 saturation.

were similar, as were the end points for each core position, suggesting that capillary trapped CO_2 is evenly distributed in the core. This is surprising, because visualization showed a significantly uneven saturation distribution during CO_2 injection (Fig. 5). A redistribution of CO_2 may have occurred during shut-in, before the second waterflood. The CO_2 saturation was high during shut-in, and it is likely that capillary redistribution of water by spontaneous imbibition (from high-saturation to low-saturation pores) forced CO_2 to spread out within the core. Saturation redistribution during the period of shut-in cannot be identified by PET due to loss of signal as ^{11}C decays. Redistribution of CO_2 during core shut-in (no injection) likely had a positive effect on the relatively high degree of capillary trapped gas, as CO_2 appeared to be more uniformly distributed in the core plug at the onset of brine injection than immediately after CO_2 injection. Capillary trapping of CO_2 has been proposed as the most rapid and effective way to ensure safe storage of CO_2, and can be controlled by waterflooding (Qi et al., 2008).

3.4. μPET addition to global data

Global measurements of pressure and produced effluents, used in most laboratory core floods, yield important information and provide the basis for assessing average system properties. Differential pressure measurements for each injection are provided in Fig. 8. The differential pressure quickly reached plateau and remained stable during the first brine injection, when the core was fully saturated by water. During CO_2 injection and second brine injection, two phases were present in the pore space: hence, the pressure increased more slowly, reached a peak value and decreased to a stable value towards the end of injection when the

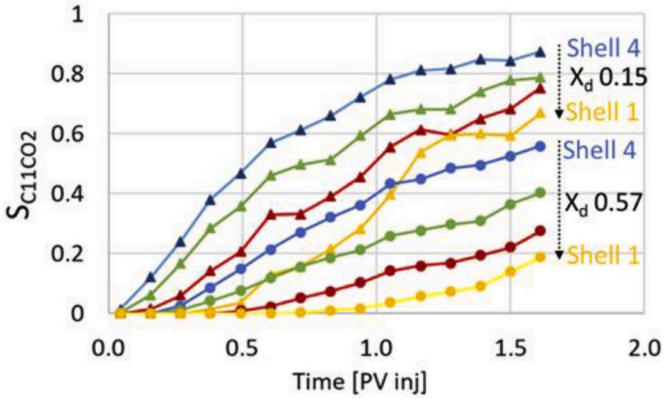

Fig. 6. Sub-core saturation development for core lengths 0.15 and 0.57 during CO_2 injection. The saturation development in shell 1 (inner core) is slower further into the core, and a wide variation in saturation end points were observed.

core saturation was stable. End point relative permeabilities can be calculated from the stabilized pressures at the end of each injection, and was 0.02 for CO_2 at the irreducible water saturation (CO_2 is the flowing phase, water is immobile). Low relative permeabilities for CO_2 were also previously observed (Busch and Müller, 2011). The end point relative permeability for water flowing through a partially CO_2-saturated core (presence of residually trapped CO_2) was 0.74.

Dynamic development of core saturation may also be determined from effluent measurements, although the inherent uncertainty may be high depending on the chosen laboratory method. *In-situ* imaging by PET provides spatially and temporally accurate saturation snap-shots (Fig. 9), where the resolution is not pre-determined but set during post-processing of the PET signal. Effluent measurements would show the deviation from ideal displacement early on during the first miscible brine and gaseous CO_2 floods, and the close to ideal development when brine was injected to trap CO_2, but without determining the cause for deviations. PET imaging revealed severe displacement heterogeneities during the first miscible brine injection and CO_2 injection, which could be quantified by sub-core analysis and attributed to a permeability variation within the chalk core. The high spatial resolution of μPET provided a sufficient number of voxels (each of 0.4 mm^3 volume) for sub-core analysis: ranging from 67 (shell 1) to 550 (shell 4), which is necessary to account for natural fluctuations in the PET instrument. For clinical PET scanners with lower spatial resolutions (2–3 mm), the same sub-core analysis would include only a few voxels and, hence, be more influenced by uncertainties. Although longitudinal discrepancies could be quantifiable, the radial displacement heterogeneities would not.

A clear advantage of most clinical PET scanners that must not be overlooked is the combination with another imaging modality, like CT or MRI: which may be used to gain insight into heterogeneities in the rock structure. CT included in preclinical μPET scanners are usually intended for small, less dense animals, hence the beam strength is not sufficient to accurately reproduce rock structure. Some structural information may, however, be available from PET imaging alone, as demonstrated during miscible brine-brine displacement.

By investigating flow dynamics in complex flow systems, such as carbonates, controlling mechanisms of CO_2 migration may be further mapped on larger scales. The possibility of using μPET to explicitly image fluid flow, and accurately quantify flow dynamics on mm-scale, unlocks significant potential in experimental work related to CO_2-EOR

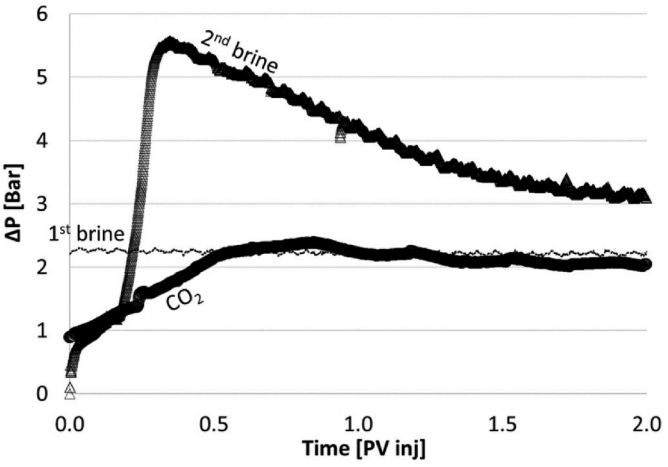

Fig. 8. Differential pressure development during brine injection when the core was fully water saturated, drainage by CO_2 and second water imbibition.

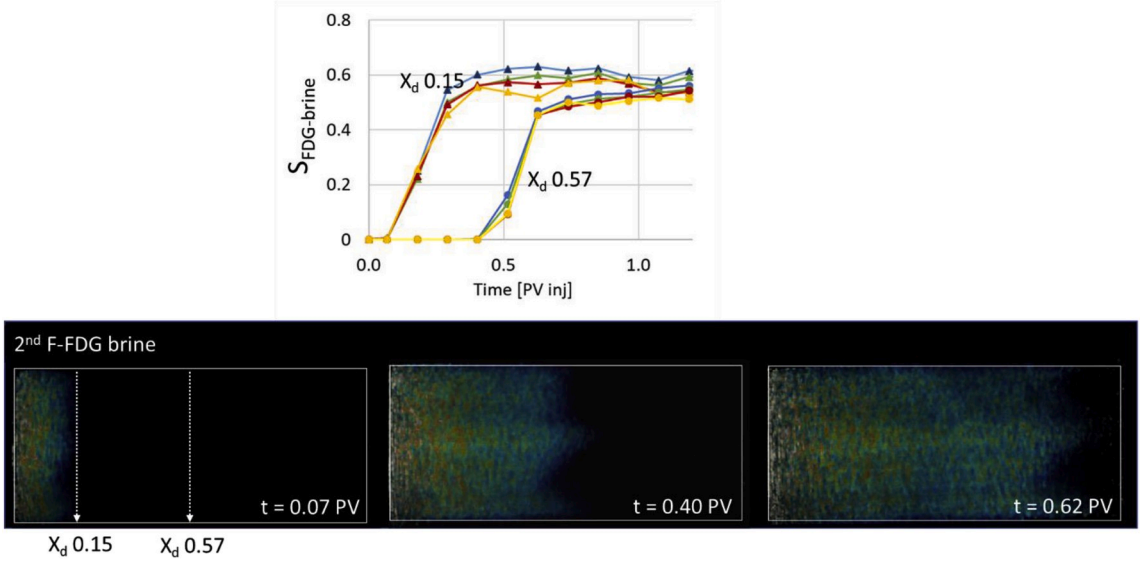

Fig. 7. Top: Sub-core saturation development for core lengths 0.15 and 0.57 during subsequent waterflooding, efficiently trapping CO_2. Bottom: 2D representation of core scale saturation development. No significant radial displacement differences were observed. Thus, during subsequent brine injection, an ideal and piston-like displacement was observed on the core and sub-core scales.

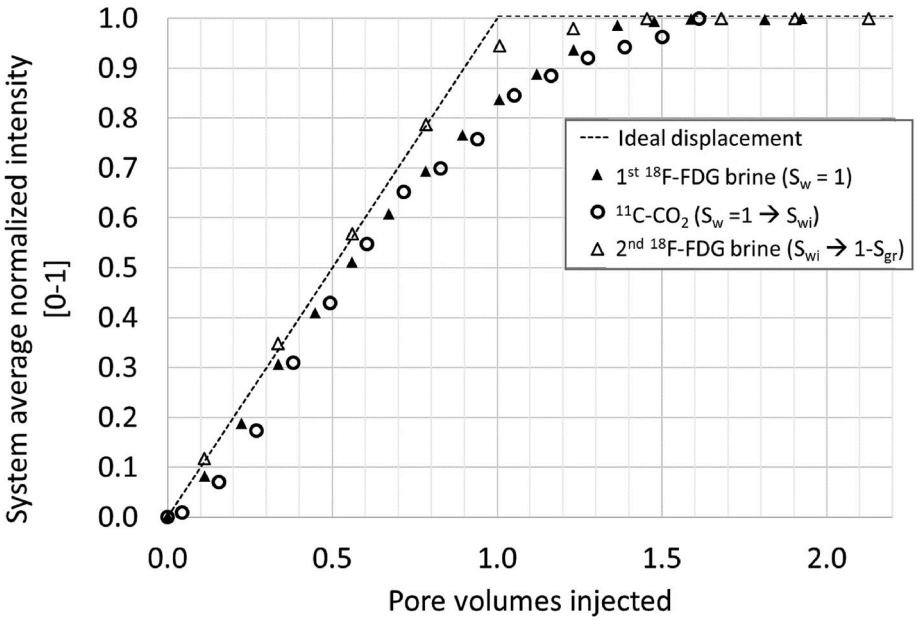

Fig. 9. Core scale saturation development from PET-imaging. The straight, dotted line shows an ideal displacement. The first brine injection and CO_2 injection deviates from ideal displacement early on, while the second brine injection (brine displacing CO_2) shows close to ideal development.

and storage. CO_2 capillary threshold pressure was previously measured using PET-imaging (Fernø et al., 2015a) and CO_2/brine relative permeabilities may be derived from unsteady-state core floods similar to the ones presented here. Positron Emission Tomography hence present a robust imaging approach to improve laboratory measurements that are important to geological CO_2 storage.

4. Conclusions

This paper demonstrated explicit and dynamic imaging of CO_2 during flow through a low-permeable chalk core at elevated pressure conditions. Short-lived radioisotopes were used to track the water and gas phases.

- Improved spatial resolution offered by preclinical μPET provided accurate quantification of spatial phase saturations during brine and CO_2 injections.
- Dynamic PET imaging revealed heterogeneous displacement patterns, which could be quantified at the mm-scale, and attributed to a sub-core variation in permeability. Sub-core permeabilities were calculated from PET displacement data.
- A CO_2 storage capacity of 66% pore volume was obtained by injecting CO_2 into a water-filled chalk core. The storage capacity was reduced to 40% after subsequent injection of water, which trapped and evenly distributed CO_2 in the pore volume.
- PET imaging may contribute to improved determination of basic flow parameters and saturation functions from core-scale experiments, which are essential to numerical simulations of CO_2 migration in the subsurface.

Declaration of competing interest

The authors declare that they have no known competing financial interests or personal relationships that could have appeared to influence the work reported in this paper.

CRediT authorship contribution statement

Bergit Brattekås: Methodology, Visualization, Formal analysis, Writing - original draft. **Malin Haugen:** Methodology, Visualization, Writing - original draft.

Acknowledgements

The PET imaging was performed at the Molecular Imaging Center in Bergen, Norway. The authors thank Heidi Espedal and Njål Brekke for help during experiments.

The authors thank the mechanical work shop at the Dept. of Physics and Technology for constructing a custom portable trolley to house the experimental equipment. The core holder was made by RS systems (Trondheim, Norway). The authors acknowledge the research council of Norway for financial support, through the "Subsurface Carbonate CO_2 Storage and Security" project no. 280341, and for funding PhD candidate Malin Haugen.

Nomenclature

^{18}F-FDG	18F-Fluorodeoxyglucose, glucose analog and radiopharmaceutical, miscible with water
^{11}C	Radioactive isotope of carbon, used to trace CO_2
$t_{1\backslash 2}$	Half-life of the decaying radioactive isotope
K	Absolute permeability [mD]
Φ	Effective porosity: [%]
L	Core length [cm]
X_d	Dimensionless core length [0-1]
Q	Volumetric flow rate [cm^3/s]
A	Cross-sectional area of core [cm^2]
μ	Fluid viscosity [Pa·s]
S_w	Fraction of water present relative to the pore volume (water saturation)
S_g	Fraction of gas present relative to the pore volume (gas saturation)
S_{wi}	Irreducible water saturation [0-1]
S_{gr}	Residual gas saturation [0-1]
V_w	Volume of water [cm^3]

Abbreviations

CO_2	Carbon dioxide
NaCl	Sodium Chloride
$CaCl_2$	Calcium chloride

EOR	Enhanced Oil Recovery
PET	Positron Emission Tomography
μPET	micro-Positron Emission Tomography
CCUS	Carbon, Capture, Utilization and Storage
MRI	Magnetic Resonance Imaging
CT	Computed Tomography
PV	Pore Volume
ΔP	Pressure drop across the unit length

References

Akbar, M., Vissapragada, B., Alghamdi, A.H., Allen, D., Herron, M., Carnegie, A., Dutta, D., Olesen, J.-R., Chourasiya, R.D., Logan, D., Stief, D., Netherwood, R., Duffy Russell, S., Saxena, K., 2000. A Snapshot of Carbonate Reservoir Evaluation, pp. 20–41. Oilfield Review, Winter 2000-2001.

Akin, S., Kovscek, A.R., 2003. Computed Tomography in Petroleum Engineering Research, vol. 215. Geological Society, London, Special Publications, pp. 23–38.

Almenningen, S., Gauteplass, J., Fotland, P., Aastveit, G.L., Barth, T., Ersland, G., 2018. Visualization of hydrate formation during CO2 storage in water-saturated sandstone. Int. J. Greenh. Gas Contr. 79, 272–278.

Bailey, D.L., Townsend, D.W., Valk, P.E., Maisey, M.N., 2005. Positron Emission Tomography. Springer.

Brattekås, B., Eide, Ø., Johansen, S.A., Vasshus, S.S., Polden, A.G., Fernø, M.A., 2019. Foam Flow and Mobility Control in Natural Fracture Networks. Transport in Porous Media.

Brattekås, B., Seright, R.S., 2018. Implications for improved polymer gel conformance control during low-salinity chase-floods in fractured carbonates. J. Petrol. Sci. Eng. 163, 661–670.

Brattekås, B., Steinsbø, M., Graue, A., Fernø, M.A., Espedal, H., Seright, R.S., 2017. New insight into wormhole formation in polymer gel during water chase floods with positron emission tomography. SPE J. 22 (1), 32–40.

Busch, A., Müller, N., 2011. Determining CO2/brine relative permeability and capillary threshold pressures for reservoir rocks and caprocks: recommendations for development of standard laboratory protocols. Energy Procedia 4, 6053–6060.

COP21, 2015. Paris: Conference of Parties 21st Meeting in Paris in December. Accessible at: https://unfccc.int/process-and-meetings/the-paris-agreement/the-paris-agreement.

Ekdale, A.A., Bromley, R.G., 1993. Trace fossils and ichnofabric in the Kjølby gaard Marl, uppermost creataceous, Denmark. Bull. Geol. Soc. Den. 31, 107–119.

Ersland, G., Fernø, M.A., Graue, A., Baldwin, B.A., Stevens, J., 2010. Complementary imaging of oil recovery mechanisms in fractured reservoirs. Chem. Eng. J. 158 (1), 32–38.

Fernø, M.A., Gauteplass, J., Hauge, L.P., Abell, G.E., Adamsen, T.C.H., Graue, A., 2015b. Combined positron emission tomography and computed tomography to visualize and quantify fluid flow in sedimentary rocks. Water Resour. Res.

Fernø, M.A., Hauge, L.P., Rognmo, A.U., Gauteplass, J., Graue, A., 2015a. Flow visualization of CO2 in tight shale formations at reservoir conditions. Geophys. Res. Lett. 42, 7414–7419.

Føyen, T.L., Fernø, M.A., Brattekås, B., 2019. The effects of nonuniform wettability and heterogeneity on induction time and onset of spontaneous imbibition. SPE J. 24 (3), 1192–1200.

IEA, 2019. The Role of CO2 Storage. IEA, Paris. https://www.iea.org/reports/the-role-of-co2-storage.

Kulenkampff, J., Gruundig, M., Richter, M., Enzmann, F., 2008. Evaluation of positron-emission-tomography for visualisation of migration processes in geomaterials. Phys. Chem. Earth 33 (14–16), 937–942.

Levin, C.S., Hoffman, E.J., 1999. Calculation of positron range and its effect on the fundamental limit of positron emission tomography system spatial resolution. Phys. Med. Biol. 44 (3), 781–799.

Pini, R., Vandehey, N.T., Druhan, J., O'Neil, J.P., Benson, S.M., 2016. Quantifying solute spreading and mixing in reservoir rocks using 3-D PET imaging. J. Fluid Mech. 796, 558–589.

Qi, R., LaForce, T.C., Blunt, M.J., 2008. Design of Carbon Dioxide Storage in Oil Fields. SPE Annual Technical Conference and Exhibition. Society of Petroleum Engineers, Denver, Colorado, USA.

Ruth, D., Fernø, M.A., Haugen, Å., Arabjamaloei, R., Brattekås, B., 2016. Matching experimental saturation profiles by numerical simulation of combined Co-/Counter-Current spontaneous imbibition. In: International Symposium of the Society of Core Analysts, Snowmass, CO, USA.

Zahasky, C., Benson, S.M., 2018. Micro-positron emission tomography for measuring sub-core scale single and multiphase transport parameters in porous media. Adv. Water Resour. 115, 1–16.

Zahasky, C., Kurotori, T., Pini, R., Benson, S.M., 2019. Positron emission tomography in water resources and subsurface energy resources engineering research. Adv. Water Resour. 127 (May 2019), 39–52.